

## COMPARATIVE STUDY ON STEADY AND UNSTEADY HEAT TRANSFER ANALYSIS OF A SPHERICAL ELEMENT USING AIR/WATER MIST TWO-PHASE FLOW

by

**Akram ABED<sup>a,b\*</sup>, Sergey SHCHEKLEIN<sup>a</sup>, and Valery PAKHALUEV<sup>a</sup>**

<sup>a</sup> Ural Federal University named after the first President of Russia B. N. Yeltsin,  
Yekaterinburg, Russia

<sup>b</sup> University of Technology, Baghdad, Iraq

Original scientific paper

<https://doi.org/10.2298/TSCI190527055A>

*In this study, two approaches to investigating the process cooling of a heated sphere were performed using air as well as air/water mist two-phase flow. Steady-state and unsteady heat transfer analysis were compared in the terms of the average surface temperature and heat transfer rate between the sphere surfaces and the cooling fluid. When the  $Bi < 0.1$ , the temperature variation inside sphere can be neglected and the widely known lumped capacitance model can be applied to estimate the heat transfer coefficient by measuring the sphere surface temperature. The effect of the different factors such as the inlet Reynolds numbers, surface temperature and water mist rate on heat transfer characteristics are examined. The experimental results showed that the presence of water mist leads to a significant increase in heat transfer rate over the use of air coolant alone. Also, the unsteady thermal behaviors of the water mist impingement on the heated surface and dynamic-state of cooling process changing over the sphere surface were analyzed experimentally based on the unsteady surface temperature measurements. The experimental results of the unsteady heat transfer were compared to the results obtained from steady-state estimation under the corresponding surface temperature of the sphere. Moreover, the new proposed empirical correlation for the Nusselt number based on the present experimental data are given for practical uses. Results reasonably agree well within  $\pm 3.8\%$ .*

Key words: *Biot number, lumped capacitance model, sphere, unsteady-state heat transfer*

### Introduction

Owing to the growing need in many thermal and practical applications for using an extremely effective cooling technique, advanced cooling techniques are required to meet the operating conditions and developing more compact and efficient heat exchanger systems. The air cooling techniques in its current form are not sufficient to dissipate the heat loads in such systems. Water cooling techniques are also employed, which offers excellent thermal performance, compared to air cooling. However, several critical problems occur during water cooling such as the requirement of pumping power, a large quantity of water required, storage problem, and the formation of water film of the quenched surface [1, 2]. Using air/water mist with no higher than several percent of the water phase provides an excellent technique of heat

\* Corresponding author, e-mail: akraam82@yahoo.com

transfer intensification with a significant reduction in size and weight of heat exchanger modules. The application of air/water mist technique is done by injecting a very fine water droplet into air main flow. Applied air/water mist to dissipate heat offers significant potential for high-heat-flux thermal management due to the high thermal properties of air/water mist mixture relative to air alone. The main features of air/water mist cooling compared to single-phase cooling can be summarized as follows: a large amount of energy is absorbed in the form of latent heat through the evaporation process of water mist at the heated surface, increase specific heat of mixture, increase the turbulence in airside and inside the thermal boundary-layer [3]. Air/water mist cooling has been developed as an effective technique for heat transfer intensification of many industrial applications by numerous authors [1-10], through both numerical and experimental works. A computational model has been developed, and heat and mass transfer in a turbulent and laminar air/water droplet flow were numerically studied by Terekhov and Pkhomov [4, 5]. They pointed out that as the mass rate of water phase increased, heat and mass transfer intensification increased with a corresponding rise in the heat spent on the heat transfer due to the phase transition (droplet evaporation). Li and Wang [6, 7] performed a series of numerical simulations to investigate the air/water mist cooling in modern gas turbines. They showed that a small amount of water mist could increase cooling effectiveness by about 30-50% under a range of temperature, velocity, and pressure conditions. They also reported the impacts of several flow parameters, water phase mass rate and injection hole configuration on the cooling effectiveness. Dhanasekaran and Wang [8] numerically and experimentally studied the single-phase as well as air/water mist two-phase flow with smooth and ribbed channels. The obtained results indicated that the mist cooling enhancement is about 30% with 2% water mist injection at the trailing surface and about 20% at the leading surface. In the second passage, 20% enhancement is predicted for both surfaces. Allais *et al.* [9] and Allais and Alvarez [10] experimentally investigated the heat transfer rate from a packed bed using a water mist with 8  $\mu\text{m}$  droplets diameter. The experiments were performed in low main flow velocity, low water mass rate and limited ranges of temperature difference. They reported that the thermal enhancement factor increased with increasing water mass rate by about 2.8 times and heat flux increased with increasing main flow velocity. For mist-cooled heat exchanger, Hayashi *et al.* [11, 12] conducted an experimental investigation of tube bundle heat exchanger a smooth and rough surface structure under steady-state conditions. They pointed out that the heat exchanger performance is sensitive to the water mass rate due to the latent heat of water mist evaporative and the effect of the wet zone extending to the rear part. All these studies have made a great contribution to developing and understanding the heat transfer mechanism. However, the effect of various water mist rates and initial heating temperatures on unsteady heat transfer has not been reported in the literature. In view of this, an experimental investigation to quantify the unsteady heat transfer behavior of a heated spherical element cooled using an air/water mist two-phase flow was performed. The surface temperature – cooling time profile was measured and analyzed. In addition, the lumped capacitance model (LCM) based on the experimental approach was adopted as a heat transfer measurement model. A steady-state heat transfer analysis has also conducted by supplying the constant heat flux on the sphere surface. The influence of water mist rate,  $j$ , surface temperature,  $T_s$ , and inlet Reynolds numbers on the mechanism of heat transfer were examined.

### Theory

When the heated sphere is exposed to an air-water mist flow, unsteady heat conduction occurs inside the sphere, whose temperature decreases with time. For small Biot numbers

the temperature variation inside the sphere can be assumed spatially uniform and a single temperature,  $T_s$ , can be appointed to clarify the time progress of heat transfer between the sphere surface and cooling fluid. Indeed, the temperature variation inside the sphere would depend on the thermal conductivity,  $k$ , of the sphere material and the heat transfer rate from the sphere surface to the cooling fluid. Due to the small heat transfer resistance inside sphere compared with the convection heat transfer resistance occurs between the sphere surface and cooling fluid, the temperature variation inside sphere can be neglected and the widely known LCM can be applied. Based on this assumption, the heat conduction equation (or global energy balance equation) can be written:

$$\rho_s V_s C_s \frac{\partial T}{\partial \tau} = \alpha A_s (T_s - T_{in}) \quad (1)$$

where  $\alpha$  is the convection heat transfer coefficient,  $T_{in}$  – the inlet fluid temperature,  $T_s$  – the temperature inside the sphere,  $\tau$  – the time, and  $\rho_s$ ,  $V_s$ ,  $C_s$ , and  $A_s$  are the density, volume, specific heat, and total surface area of sphere, respectively. The analytical solution of eq. (1) can be obtained [13]:

$$\alpha = \frac{C_p \rho d_{sp}}{6} \sum_{i=1}^n \left[ \frac{1}{\Delta \tau} \ln \left( \frac{T_{s,i} - T_{in}}{T_{s,i+1} - T_{in}} \right) \right] \quad (2)$$

where  $T_s$  is the higher temperature of the sphere's surface,  $T_{s+j+1}$  – the lower temperature of the sphere's surface, and  $\tau$  – the time difference between two readings of the data logger. Basically, the LCM is appropriate to systems of a Biot number ( $Bi < 0.1$ ) [13], where Biot number is defined:

$$Bi = \frac{\alpha L}{\lambda_s} \quad (3)$$

where  $\lambda_s$  is the thermal conductivity of the sphere and  $L$  – the characteristic dimension of the sphere, defined as the ratio between the sphere volume,  $V_s$ , and its total surface area,  $A_s$ . The properties of sphere material as a heat transfer test object are.

- thermal conductivity:  $\lambda_s = 400$  W/mK,
- density:  $\rho_s = 9723.32$  kg/m<sup>3</sup>, and
- specific heat:  $C_s = 390$  J/kgK.

Under the work conditions, the Biot number is about 0.001-0.009. Next, a steady-state heat transfer was also performed by supplying the constant heat flux on the sphere surface by using a 100 W cartridge heater having tube-shape with 0.031 m length and 0.008 m diameter. The input power was adjusted using a variac voltage regulator so as to achieve the required surface heat flux (12831 W/m<sup>2</sup>). It can be estimated as [14]:

$$q'' = \frac{Q_{el} - Q_{los}}{A_s} \quad (4)$$

where  $Q_{el}$  is the input electrical power to the test sphere and  $Q_{los}$  – the heat loss. In the present study, the air, as well as air/water mist used as cooling fluids. The water droplets trajectory can be predicted by applying Newton's second law. The governing equations for the water droplets [15]:

$$\frac{dm_p}{d\tau} = -\alpha_m A_p (\rho_{v,s} - \rho_v) \quad (5)$$

$$\frac{du_p}{d\tau} = \frac{18\mu}{\rho_p D_p^2} \frac{C_p \text{Re}}{24} (u - u_p) \quad (6)$$

$$m_p C_p \frac{dT}{d\tau} = \pi d^2 \alpha (T_{\text{ave.s}} - T_{ia}) + \frac{dm_p}{d\tau} h_{fg} \quad (7)$$

where  $\alpha_m$  is the mass transfer coefficient,  $h_{fg}$  – the latent heat of evaporation,  $D_p$  – the water droplet diameter, and  $A_p$  – the surface area of the droplet. The Reynolds number is defined:

$$\text{Re} = \frac{\rho u D}{\mu} \quad (8)$$

Lang [16] formula was adopted to estimate the water droplet diameter:

$$D_p = 0.34 \left( \frac{8\pi\sigma}{\rho F^2} \right)^{1/3} \quad (9)$$

The dimensionless Weber number is defined:

$$\text{We} = \frac{j^2 D_p}{2\rho_w \sigma} \quad (10)$$

The water phase transition,  $K$ , can be estimated:

$$K = \frac{h_{fg}}{C_p (T_s - T_\infty)} \quad (11)$$

### Experimental set-up and procedure

The experimental set-up is shown schematically in fig. 1. This set-up enables to investigate the average heat transfer of a sphere placed inside a cylindrical channel in unsteady heat transfer conditions. For steady-state conditions, the experimental test-bench and the test sphere are similar as described in our previous paper [17]. On the side of the unsteady conditions, a 34 mm diameter copper sphere with a smooth heating surface was used in the experiment runs. A non-contact high-frequency induction heating station was used to heat the test sphere with a copper helical coil to appropriate work at frequencies between 50-100 KHz. The induction coil of inner diameter 55 mm was made from 8 mm O. D. (copper tubing). The coil had 2 turns and the connection of the coil to the induction circuit was made with two 200 mm lengths of copper tubing spaced 50 mm apart. The induction coil was positioned directly around the test sphere being heated. Sphere after heating in the high-frequency induction heating station was exposed to air as well as air/water droplet flow. In this study, the oxidation influence could be ignored due to the slight effect on the surface thermal conductivity. The initial temperature of the test object was  $T_{si} = 100$  °C, 200 °C, and 300 °C. The temperature of the sphere and cooling fluid were measured with two calibrated, fast response  $K$ -type thermocouples were implanted inside the sphere. The surface, ambient, cooling fluid temperatures and cooling downtime were recorded constantly. All thermocouples are connected to the data acquisition system that consists of an analog signal input type OWEN MV110-8A with MSD200 data logger. The water mist system was a 1.7 MHz ultrasonic mist generator has the same structure as the one used in [16]. This type of mist generator was chosen due to the low power consumption and quiet operation

comparing with other mist and evaporative generators. To perform this study, the following procedure was generally followed: firstly the test object is heated by the induction heat station. The induction station was switched on and the input power was adjusted to achieve the required temperature. When the surface temperature was achieved, the induction station was switched off and the test object was exposed to air as well as air/water mist two-phase flows. The temperature of the test object by means of a digital data logger with 10 second intervals is measured respectively. All experiments were performed several times to reduce an error for each temperature cases. The deviation was varied from 2% to 8%.

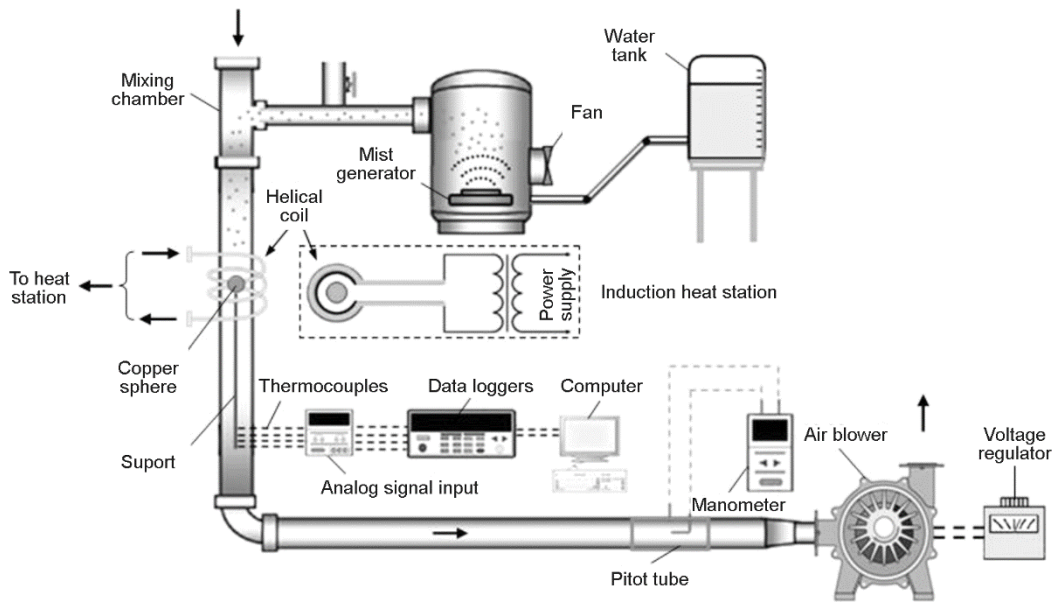


Figure 1. Schematic diagram of the experimental set-up

### Error analysis and uncertainty

In the steady and unsteady heat transfer experiments, the air velocity, temperature, and water mass-flow rate were measured using appropriate instruments. The reliability of experimental data has been presented by uncertainty calculations as discussed in [18, 19]. The uncertainties of non-dimensional parameters (Nu, Re) and measurement were evaluated and given in tab. 1.

$$\left(\frac{\Delta \text{Nu}}{\text{Nu}}\right)^2 = \frac{1}{\text{Nu}} \left\{ \left[ \frac{\partial}{\partial \alpha} (\text{Nu}) \Delta \alpha \right]^2 + \left[ \frac{\partial}{\partial d_s} (\text{Nu}) \Delta d_s \right]^2 + \left[ \frac{\partial}{\partial \lambda_s} (\text{Nu}) \Delta \lambda_s \right]^2 \right\} \quad (12)$$

$$\left(\frac{\Delta \alpha}{\alpha}\right)^2 = \frac{1}{\alpha} \left\{ \left[ \frac{\partial}{\partial q''} (\alpha) \Delta q'' \right]^2 + \left[ \frac{\partial}{\partial T_{\text{ave},s}} (\alpha) \Delta T_{\text{ave},s} \right]^2 + \left[ \frac{\partial}{\partial T_{ia}} (\alpha) \Delta T_{ia} \right]^2 \right\} \quad (13)$$

$$\left(\frac{\Delta \text{Re}}{\text{Re}}\right)^2 = \frac{1}{\text{Re}} \left\{ \left[ \frac{\partial}{\partial u} (\text{Re}) \Delta u \right]^2 + \left[ \frac{\partial}{\partial \rho} (\text{Re}) \Delta \rho \right]^2 + \left[ \frac{\partial}{\partial D} (\text{Re}) \Delta D \right]^2 + \left[ \frac{\partial}{\partial \mu} (\text{Re}) \Delta \mu \right]^2 \right\} \quad (14)$$

**Table 1. Uncertainty in experimental instruments**

| Instrument           | Error [%]           |
|----------------------|---------------------|
| Thermocouple, K-type | 0.9                 |
| Bitot tube           | 1.25                |
| Digital manometer    | 0.3                 |
| Parameter            | Maximum uncertainty |
| Nusselt number       | 4                   |
| Reynolds number      | 1.91                |

## Results and discussion

### Confirmatory test of the sphere for a single phase – air coolant

In the following section, the experimental results of the single-phase air cooling under steady-state conditions are reported to confirm the reliability of the experimental facility.

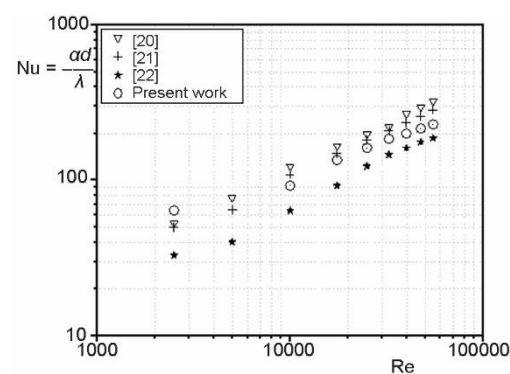


**Figure 2. A comparison of the average Nusselt number from literature with results from the present study for sphere at different Reynolds numbers**

The heat transfer characteristics in the terms of Nusselt number with Reynolds number are validated as shown graphically in fig. 2. The average Nusselt number obtained from the present work are compared with the correlations of Achenbach [20], Romkes *et al.* [21], and Whitaker *et al.* [22].

The comparison exhibits the present results are in good agreement with those from the empirical correlations. This demonstrates that the process applied and experimental facility in the present work is reliable. With the help of the experimental data, the following empirical correlation was derived:

$$Nu = 0.47 Re^{0.58} Pr^{0.33} \quad (15)$$

### Steady-state heat transfer characteristics

The results of the average surface temperature and heat transfer coefficient for a single-phase air-flow and range of water mist rate are shown in figs. 3 and 4. It can be seen that in fig 4, the average surface temperature in single-phase air-flow tends to decrease gradually by increasing the Reynolds number. When the heated sphere exposed to air/water mist two-phase flow, the effect of water mist evaporation appears and can be noticed that the surface temperature decreases as water mist rate increases for constant heat flux. It is worth noting that, when the surface temperature is high ( $T_s \leq 280$  °C), the water mist may be evaporated completely before reaching at the heated surface due to the force of evaporation, resulting to significantly reduce the sensible heat of the air-flow and formation an air-vapor medium near the sphere surface and inside the thermal boundary-layer. On the other hand, at a low surface temperature ( $T_s \leq 60$  °C), most of the heated surface becomes available for wetting and form a liquid film. The results obtained from the related experimental work revealed that the pres-

ence of water mist leads to a significant decrease in surface temperature by about 6.7%, 25%, 45%, and 51% compared with air-cooling under different water mist rates.

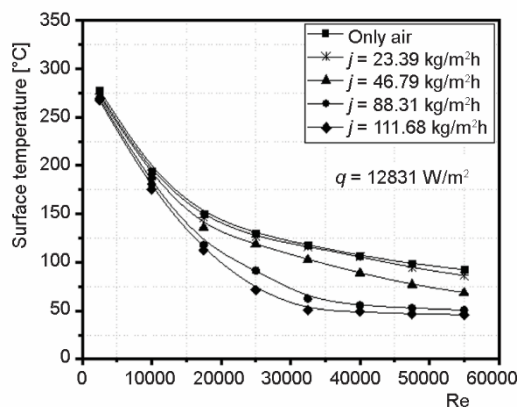


Figure 3. Variations of the average surface temperature as a function of Reynolds number

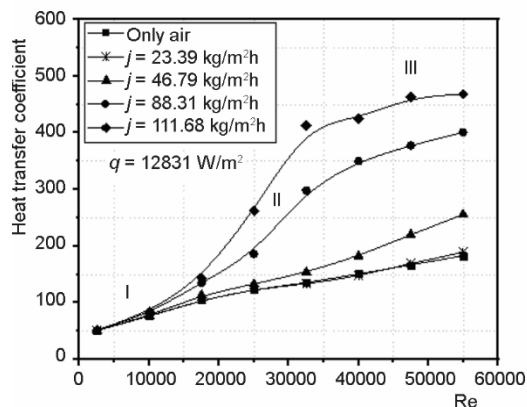


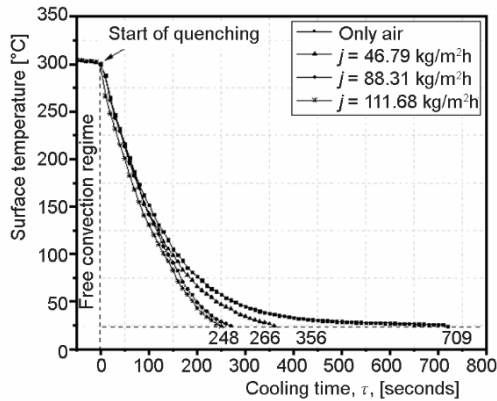
Figure 4. Variations of the average heat transfer coefficient as a function of Reynolds number; I – dry region, II – dryout region, III – wet region

Figure 4 depicts the experimental results for the average heat transfer coefficient as a function of the Reynolds number for a range of water mist rate. The average heat transfer coefficient of air/water mist flow are, respectively, 1%, 19.7%, 90.2%, and 134% higher than those in the single-phase for a range of water mist rate ( $j = 23.39-111.68 \text{ kg/m}^2$  per hour). For Reynolds numbers varied from 30000 to 55000, the average heat transfer coefficient significantly increases under range of water mist rate ( $j = 88.31-111.68 \text{ kg/m}^2$  per hour) and it can be explained as follows: with increasing  $j$ , the surface wetting increases and approximately reaches 30% by formation of liquid film that ultimately enhances the heat transfer rate due to the release of evaporative latent heat. For the case of the Reynolds numbers varied from 17500 to 30000, the tendency of heat transfer increase is different from that of the high Reynolds numbers. However, the water mist reaching to the heated surface, but evaporates immediately in the heated surface without liquid films formed. As the surface temperature increases ( $Re \leq 17500$ ), the heat-transfer coefficient decreases due to water mist vaporization without wetting the heated surface. An empirical correlation for heat transfer rate in the terms of Nusselt number was developed in the present work, in which the dimensionless Reynolds number, Weber number, and the parameter of the water phase transition,  $K$ , was taken into account as shown below. The absolute deviations between the experimental and predictions data are 3.8%.

$$Nu = 2.59 Re^{0.66} We^{0.14} K^{0.152} \quad (16)$$

#### Unsteady-state heat transfer characteristics

Herein, the unsteady surface temperature acquired by implanted thermocouples at the sphere center was used as reference data to estimate the surface temperature profile during air/water mist cooling process. Air/water mist cooling was performed with an initial surface temperature  $T_{si} = 100 \text{ }^\circ\text{C}$ ,  $200 \text{ }^\circ\text{C}$ , and  $300 \text{ }^\circ\text{C}$  and range of Reynolds numbers. Figure 5 depicts the temperature profile (quench curve) with the initial temperature equal to  $300 \text{ }^\circ\text{C}$  for a



**Figure 5. Unsteady cooling curves for different water mist rate at  $Re = 55000$**

300 °C to 24 °C under constant Reynolds number ( $Re = 55000$ ).

The variation of temperature profile with cooling time under different Reynolds numbers are also reported and analyzed as shown in fig. 6. In each figure, the presented surface temperatures are the values connected to the corresponding Reynolds number under constant water mist rate. It can be seen that, as Reynolds numbers increases, the surface cooling time decreases under constant water mist rate. It is noticed that surface temperature is a strong function of water mist rate and Reynolds numbers where  $T_s$  decreases with increases in water mist rate and Reynolds numbers. For  $j = 88.31 \text{ kg/m}^2$  per hour, the cooling time of  $Re = 55000$ ,  $Re = 40000$ ,  $Re = 25000$ , decreased by 167%, 126%, and 122%, respectively, from corresponding cooling time by  $j = 0$ . In the present study, high Reynolds number means high main flow velocity which drives more and more water mist to reach the heated surface and absorbs a large amount of energy in the form of latent heat during the evaporation process. Based on the sphere surface temperature and the direct observation method through a glass transparent channel with the help of a video camera, it can be classified the cooling curve into three different stages such as I – dry region, II – dry-out region, and III – wet re-

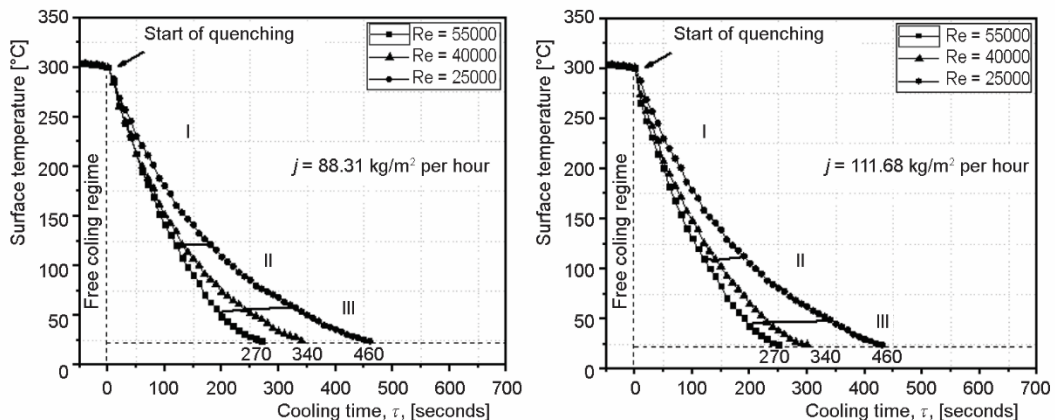


**Figure 6. Influence of the Reynolds number on the surface temperature**

varied range of air/water mist rate. Two distinctive regimes of heat transfer can be observed in fig 5. At the starting of the cooling process, the temperature drops by around 5 °C connected to the loss of heat due to the free convection and radiation which occurs during the air/water mist system adjustment to achieve the required water mist before the cooling process starts. Next, heat loss occurs due to air/water mist cooling. The cooling time from 300 °C to 24 °C is found to be 709, 356, 266, and 248 seconds for air cooling and a varied range of air/water mist rate. The cooling time for  $j = 46.79$ ,  $88.31$ , and  $111.68 \text{ kg/m}^2$  per hour is found to be 49.78, 62.4, and 65 times less compared to the cooling time with  $j = 0$  for cooling the sphere from

gion. In the region -I, when the surface temperature is high, the water mist comes in non-contact with the heated surface and the water mist completely evaporates near the sphere surface and inside the thermal boundary-layer. Region-II occurs when the water mist comes in contact with the heated surface and water mist immediately evaporates.

In this stage, the liquid film does not form on the heated surface due to the high surface temperature and high velocity of air that sweeps away the partly evaporated water mist before they get accumulated on the heated surface. Region-III occurs after the surface wetting phenomenon, due to the lower surface temperature. Figure 7 depicts the experimental results for the average heat transfer coefficient as a function of cooling time for a range of Reynolds number under constant water mist rate. For all cases, the heat transfer coefficient was increased with increasing of water mist rate. Also, it can be seen that the heat transfer coefficient was increased with increasing of Reynolds number due to the increase of turbulent intensity, resulting in more efficient destruction of the thermal boundary-layer.

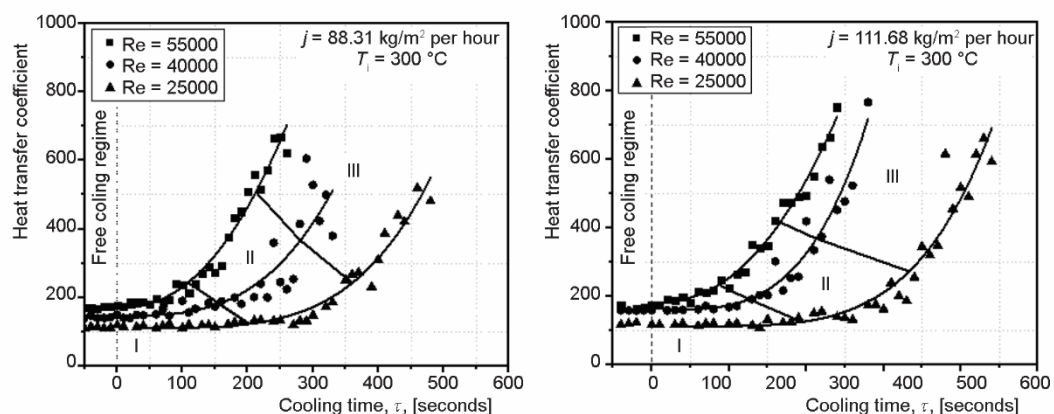
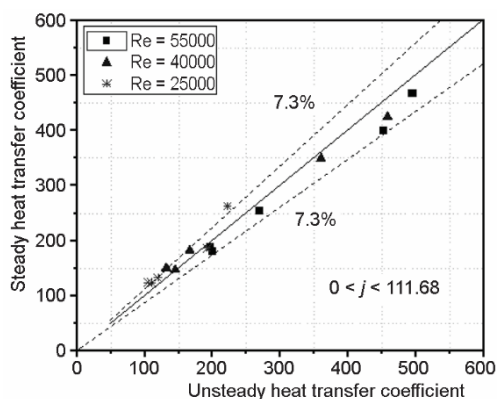


Figure 7. Heat transfer coefficient for different Reynolds numbers and range of water mist rate

The heat transfer mechanism due to water mist impingement on the heated surface can be classified into three important physical regimes. Regime I can be specified as a clear convection regime, corresponds to the dry region (region I). Regimes II and III, can be identified as convection and evaporation regimes, corresponds to the dry-out and wet regions (region II and III). It is noticed that the highest value of heat transfer coefficient is obtained by supplying the higher value of water mist rate. The maximum heat transfer coefficient is at the wet region (Regime III) and decreases as surface temperature increases. The heat transfer coefficient is found to be 228, and 179.4 times higher compared to the heat transfer coefficient with  $Re = 25000$  for  $j = 111.68 \text{ kg/m}^2 \text{ per hour}$  at  $\tau = 200$  seconds.

#### Validation of the LCM model proposed

The unsteady heat transfer was carried out for a varied range of water mist rate and different values of Biot numbers using LCM solutions for the surface temperature of the sphere (for the chosen Reynolds numbers) as conditions. Results of heat transfer coefficient measured by steady-state conditions are compared with the results obtained by LCM in terms of corresponding surface temperature of the sphere. The heat transfer coefficient of the LCM is obtained by solving the corresponding equation, *i. e.*, eq. (2) for  $T_s = 300\text{-}24 \text{ }^\circ\text{C}$ . The com-



**Figure 8.** Comparison of steady heat transfer coefficient with those obtained by the LCM under corresponding surface temperature

parison between the steady and unsteady heat transfer characteristics is shown graphically in fig. 8. In this figure, results reasonably agree well within  $\pm 7.3\%$ .

### Conclusion

An experimental investigation was performed to predict the thermal behavior of a sphere cooling process with steady- and unsteady-state heat transfer conditions. The LCM was adopted with an aim to investigate the average heat transfer coefficient ( $Nu$ ) of the sphere cooling by using air as well as air/water mist two-phase flow. The effect of the different factors such as the inlet Reynolds numbers, surface temperature and water mist rate on heat transfer characteristics are examined. From the

obtained results, an extremely effect of water mist is observed on the heat transfer characteristics. The average heat transfer coefficient of air/water mist flow are respectively 1%, 19.7%, 90.2%, and 134% higher than those in the single-phase air cooling for a range of water mist rate ( $j = 23.39 \sim 111.68$  kg/m<sup>2</sup> per hour). The heat transfer mechanism due to water mist impingement on the sphere surface was analyzed and classified into three important physical regimes. Regime-I specified as a clear convection regime, corresponds to the dry region. Regimes II and III, can be identified as convection and evaporation regimes, corresponds to the dry-out and wet regions. Moreover, the new proposed empirical correlation for the Nusselt number based on the present experimental data are given for practical uses. The agreement between the results obtained from the experimental data and those obtained from the proposed correlation is reasonable.

### Nomenclature

$A$  – area, [m<sup>2</sup>]  
 $Bi$  – Biot number, [-]  
 $C$  – specific heat, [Jkg<sup>-1</sup>K<sup>-1</sup>]  
 $C_p$  – specific heat at constant pressure, [Jkg<sup>-1</sup>K<sup>-1</sup>]  
 $D$  – diameter, [m]  
 $d_{sp}$  – diameter of a sphere, [m]  
 $F$  – ultrasonic frequency, [Hz]  
 $h_{fg}$  – latent heat of water evaporation, [kJkg<sup>-1</sup>]  
 $j$  – water mist rate, [kgm<sup>-2</sup>h<sup>-1</sup>]  
 $L$  – characteristic dimension, [m]  
 $m_p$  – mass of water drop, [kgm<sup>-3</sup>]  
 $Nu$  – Nusselt number, [-]  
 $Q_{el}$  – input electrical power, [W]

$Q_{los}$  – heat loss, [W]  
 $q''$  – heat flux, [Wm<sup>-2</sup>]  
 $Re$  – Reynolds number, [-]  
 $T$  – temperature, [°C]  
 $u$  – velocity, [ms<sup>-1</sup>]

### Greek letter

$\alpha$  – heat transfer coefficient, [Wm<sup>-2</sup>K<sup>-1</sup>]  
 $\lambda$  – thermal conductivity, [Wm<sup>-1</sup>K<sup>-1</sup>]  
 $\mu$  – dynamic viscosity, [kgm<sup>-1</sup>s<sup>-1</sup>]  
 $\rho$  – density, [kgm<sup>-3</sup>]  
 $\sigma$  – surface tension, [Nm<sup>-1</sup>]

### References

- [1] Sharma, A., Sahu, S., An Experimental Study on Heat Transfer and Rewetting Behavior of Hot Horizontal Downward Facing Hot Surface by Mist Jet Impingement, *Applied Thermal Engineering*, 151 (2019), Mar., pp. 459-474
- [2] Zhong, Y., et al., CFD Simulation on the Flow and Heat Transfer Characteristics of Mist Flow in Wire-Wrapped Rod Bundle, *Nuclear Engineering and Design*, 345 (2019), Apr., pp. 62-73

- [3] Wang, T., Dhanasekaran, T., Calibration of a Computational Model to Predict Mist/Steam Impinging Jets Cooling With an Application to Gas Turbine Blades, *Journal of Heat Transfer*, 132 (2010), 12, pp. 122201-122211
- [4] Terekhov, V., Pakhomov, M., Numerical Study of Heat Transfer in a Laminar Mist Flow Over a Isothermal Flat Plate, *International Journal of Heat and Mass Transfer*, 45 (2002), 10, pp. 2077-2085
- [5] Terekhov, V., Pakhomov, M., Numerical Simulations of Hydrodynamics and Convective Heat Transfer in a Turbulent Tube Mist Flow, *International Journal of Heat and Mass Transfer*, 46 (2003), 9, pp. 1503-1517
- [6] Li, X., Wang, T., Simulation of Film Cooling Enhancement With Mist Injection, *Journal of Heat Transfer*, 128 (2006), 6, pp. 509-519
- [7] Li, X., Wang, T., Effects of Various Modeling Schemes on Mist Film Cooling Simulation, *Journal of Heat Transfer*, 129 (2007), 4, pp. 472-482
- [8] Dhanasekaran, T., Wang, T., Computational Analysis of Mist/Air Cooling in a Two-Pass Rectangular Rotating Channel with 45-deg Angled Rib Turbulators, *International Journal of Heat and Mass Transfer*, 61 (2013), June, pp. 554-564
- [9] Allais, I., et al., Modelling Cooling Kinetics of a Stack of Spheres During Mist Chilling, *Journal of Food Engineering*, 72 (2006), 2, pp. 197-209
- [10] Allais, I., Alvarez, G., Analysis of Heat Transfer During Mist Chilling of a Packed Bed of Spheres Simulating Foodstuffs, *Journal of Food Engineering*, 49 (2001), 1, pp. 37-47
- [11] Hayashi, Y., et al., Study on Mist Cooling for Heat Exchangers, 3rd report, Development of High-Performance Mist Cooled Heat Transfer Tubes, *Transactions of the Japan Society of Mechanical Engineers Series B*, 54 (1988), 505, pp. 2617-2623
- [12] Hayashi, Y., et al., Heat Transfer from Tubes in Mist Flows, *Experimental Heat Transfer*, 4 (1991), 4, pp. 291-308
- [13] Lienhard V. J. H., Lienhard IV. J. H., *A Heat Transfer Textbook*, Dover Publications, Mineola, N. Y., USA, 2013
- [14] Quinn, C., et al., Heat Transfer Behaviour of a Dilute Impinging Air-Water Mist Jet at Low Wall Temperatures, *International Journal of Heat and Mass Transfer*, 111 (2017), Aug., pp. 1234-1249
- [15] Kumari, N., et al., Analysis of Evaporating Mist Flow for Enhanced Convective Heat Transfer, *International Journal of Heat and Mass Transfer*, 53 (2010), 15-16, pp. 3346-3356
- [16] Lang, R. J., Ultrasonic Atomization of Liquid, *Acoust. Soc. Am.*, 34 (1962), 1, pp. 6-8
- [17] Abed, A., et al., Investigation of Heat Transfer Coefficient of Spherical Element Using Infrared Thermography (IR) and Gas – Water Droplets (Mist) as Working Medium, *IOP Conference Series: Materials Science and Engineering*, 481 (2019), 1, ID 012033
- [18] Abernethy, R., et al., ASME Measurement Uncertainty, *Journal of Fluids Engineering*, 107 (1985), 2, pp. 161-164
- [19] Kline, S. J., McClintock, F. A., Describing Uncertainties in Single Sample Experiments, *Mechanical Engineering*, 75 (1953), pp. 3-8
- [20] Achenbach, E., Heat Transfer from Spheres up to  $Re = 6 \times 10^6$ . *Proceedings*, 6<sup>th</sup> International Heat Transfer Conference, Hemisphere, Washington, DC, 1978, 5
- [21] Romkes, S., et al., CFD Modelling and Experimental Validation of Particle-to-Fluid Mass and Heat Transfer in a Packed Bed at Very Low Channel to Particle Diameter Ratio, *Chemical Engineering Journal*, 96 (2003), 1-3, pp. 3-13
- [22] Whitaker, S., Forced Convection Heat Transfer Correlations for Flow in Pipes, Past Flat Plates, Single Cylinders, Single Spheres, and for Flow in Packed Beds and Tube Bundles, *AIChE Journal*, 18 (1972), 2, pp. 361-371